The Topology of Symmetric, Second-Order Tensor Fields

Thierry Delmarcelle

Department of Applied Physics
Stanford University
Stanford, CA 94305-4090

Lambertus Hesselink

Department of Electrical Engineering
Stanford University
Stanford, CA 94305-4035

Abstract

We study the topology of symmetric, second-order tensor fields. The goal is to represent their complex structure by a simple set of carefully chosen points and lines analogous to vector field topology. We extract topological skeletons of the eigenvector fields, and we track their evolution over time. We study tensor topological transitions and correlate tensor and vector data.

The basic constituents of tensor topology are the degenerate points, or points where eigenvalues are equal to each other. Degenerate points play a similar role as critical points in vector fields. We identify two kinds of elementary degenerate points, which we call wedges and trisectors. They can combine to form more familiar singularities—such as saddles, nodes, centers, or foci. However, these are generally unstable structures in tensor fields.

Finally, we show a topological rule that puts a constraint on the topology of tensor fields defined across surfaces, extending to tensor fields the Poincaré-Hopf theorem for vector fields.

1 Introduction

Many physical phenomena are described in terms of continuous vector and tensor data. In fluid flows, for example, velocity, vorticity, and temperature gradients are vector fields. Stresses, viscous stresses, rate-of-strain, and momentum flux density are symmetric tensor fields.

Both vector and tensor fields are multivariate; they involve more than one piece of information at every point of space. In fact, vector and symmetric tensor fields in N dimensional space embody as much information as N and $\frac{1}{2}N(N+1)$ independent scalar fields, respectively! Visualizing such data is a difficult challenge, mainly because of the necessity of rendering the underlying continuity while avoiding problems of visual clutter. (See for example Reference [1] for a unified exposé of vector and tensor visualization techniques.)

Representing vector fields by their topology is powerful at fulfilling this requirement. The topology is obtained by locating critical points—i.e., points where the magnitude of the vector field vanishes—and by displaying the set of their connecting streamlines [2, 3]. From this simple and austere depiction, an observer can infer the structure of the whole vector field.

In this article we discuss topological representations of 2-D symmetric, second-order tensor fields (referred to here simply as "tensor fields"). That is, we investigate data of the type

$$\mathbf{T}(\overline{x}) = \begin{pmatrix} T_{11}(x,y) & T_{12}(x,y) \\ T_{12}(x,y) & T_{22}(x,y) \end{pmatrix} \tag{1}$$

$\mathbf{T}(\overline{x})$ is fully equivalent to two orthogonal eigenvectors

$$\overline{v}_i(\overline{x}) = \lambda_i(\overline{x})\overline{e}_i(\overline{x}) \tag{2}$$

where $i = 1, 2$ (Figure 1). $\lambda_i(\overline{x})$ are the eigenvalues of $\mathbf{T}(\overline{x})$ and $\overline{e}_i(\overline{x})$ the unit eigenvectors. (The reader unacquainted with these concepts will find Reference [4] especially useful.) The eigenvectors $\overline{v}_i(\overline{x})$ represent all

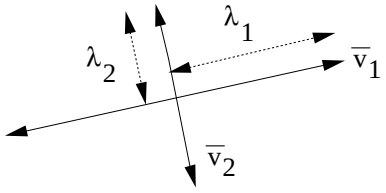

Figure 1: The two orthogonal eigenvectors $\overline{v}_i$ represented as bidirectional arrows.

the *amplitude* information ($\lambda_i(\overline{x})$) and all the *directional* information ($\overline{e}_i(\overline{x})$) represented in matrix notation by the components $T_{ij}(\overline{x})$. In a stress-tensor field, for example, the vectors $\overline{v}_i(\overline{x})$ describe the magnitude and direction of the principal stresses. We represent $\overline{v}_1$ and $\overline{v}_2$ in Figure 1 as bidirectional arrows because their sign is not determined.

To obtain continuous representations of tensor fields, we integrate a series of curves along one of the eigenvectors $\overline{v}_1(\overline{x})$ or $\overline{v}_2(\overline{x})$. We refer to these curves as "tensor

field lines" [5] or as "hyperstreamline trajectories" for consistency with our earlier work [6].

The topology of a tensor field $\mathbf{T}(\overline{x})$ is the topology of its eigenvector fields $\overline{v}_i(\overline{x})$. As with regular vector fields, we seek topological skeletons that provide simple depictions of the structure of the eigenvector fields. We obtain these skeletons by locating degenerate points (Section 2) and integrating the set of their connecting hyperstreamline trajectories (Section 3). Due to their sign indeterminacy, eigenvectors have a different structure from regular, signed vector fields. For example, we show a tensor topological rule constraining the structure of tensor fields defined across surfaces (Section 4). Finally, we discuss succinct extensions of our theory to 3-D and to unsymmetric tensor data (Section 5).

2 Degenerate Points

We build a topological analysis of tensor fields from the concept of degenerate points, which play the role of critical points in vector fields.

Streamlines in vector fields never cross each other except at critical points and, as we show below, hyperstreamlines in tensor fields meet each other only at degenerate points. Similar to critical points, degenerate points are the basic singularities underlying the topology of tensor fields. We define them mathematically as follows.

Definition 1 (Degenerate point) *A point $\overline{x}_0$ is a degenerate point of the tensor field $\mathbf{T}(\overline{x})$ iff the two eigenvalues of $\mathbf{T}(\overline{x})$ are equal to each other at $\overline{x}_0$—i.e., iff $\lambda_1(\overline{x}_0) = \lambda_2(\overline{x}_0)$.*

Let us denote by λ the common eigenvalue at the degenerate point $\overline{x}_0$. At $\overline{x}_0$, the tensor field is proportional to the identity matrix:

$$\mathbf{T}(\overline{x}_0) = \begin{pmatrix} \lambda & 0 \\ 0 & \lambda \end{pmatrix}$$

which implies that $\mathbf{T}(\overline{x}_0)\overline{e} = \lambda\overline{e}$ for every vector $\overline{e}$. At most points, there is only one eigenvector associated with each eigenvalue but, at degenerate points, there are an infinity of such eigenvectors. So hyperstreamlines cross each other at degenerate points.

Degenerate points satisfy the following conditions:[1]

$$\begin{cases} T_{11}(\overline{x}_o) - T_{22}(\overline{x}_o) = 0 \\ T_{12}(\overline{x}_o) = 0 \end{cases} \tag{3}$$

which we use to locate them. When the data are defined on a discrete grid, we use bilinear interpolation of the tensor components between vertices.

[1] Valid in any coordinate system.

2.1 Index, sectors, and separatrices

In vector fields there are various types of critical points—such as nodes, foci, centers, and saddle points—that correspond to different local patterns of the neighboring streamlines. These patterns are characterized by the vector gradients at the positions of the critical points [2].

Likewise in tensor fields, different types of degenerate points occur that correspond to different local patterns of the neighboring hyperstreamlines. These patterns are determined by the tensor gradients at the positions of the degenerate points.

Consider the partial derivatives

$$\begin{array}{ll} a = \frac{1}{2}\frac{\partial(T_{11}-T_{22})}{\partial x} & b = \frac{1}{2}\frac{\partial(T_{11}-T_{22})}{\partial y} \\ c = \frac{\partial T_{12}}{\partial x} & d = \frac{\partial T_{12}}{\partial y} \end{array} \tag{4}$$

evaluated at the degenerate point $\overline{x}_0$. In the vicinity of $\overline{x}_0$, we can expand tensor components to first-order as

$$\begin{cases} \frac{T_{11}-T_{22}}{2} \approx a\Delta x + b\Delta y \\ T_{12} \approx c\Delta x + d\Delta y \end{cases} \tag{5}$$

where $(\Delta x, \Delta y)$ are small displacements from $\overline{x}_0$. An important quantity for the characterization of degenerate points is

$$\delta = ad - bc \tag{6}$$

The appeal of δ arises from its being invariant under rotation. That is, if you rotate the coordinate system, both tensor components T_{ij} and partial derivatives $\{a, b, c, d\}$ change, but δ remains constant [7].

To proceed further we define the concept of an *index at a degenerate point*. This extends from vector fields to tensor fields the classical notion of an index at a critical point [8].

Definition 2 (Tensor index) *The index at the degenerate point $\overline{x}_0$ of a tensor field is the number of counter-clockwise revolutions made by the eigenvectors when traveling once in a counter-clockwise direction along a closed path encompassing $\overline{x}_0$. The path is chosen close enough to $\overline{x}_0$ so that it does not encompass any other degenerate points.*

While indices at critical points of continuous vector fields must be integer quantities (1 for a node, -1 for a saddle, etc.), indices at degenerate points of continuous tensor fields are half-integers. This arises from the sign ambiguity of the eigenvectors. In fact, we show in Reference [7] that, *if $\delta \neq 0$, the index I at $\overline{x}_0$ is given by*

$$I = \frac{1}{2}sign(\delta) = \pm\frac{1}{2} \tag{7}$$

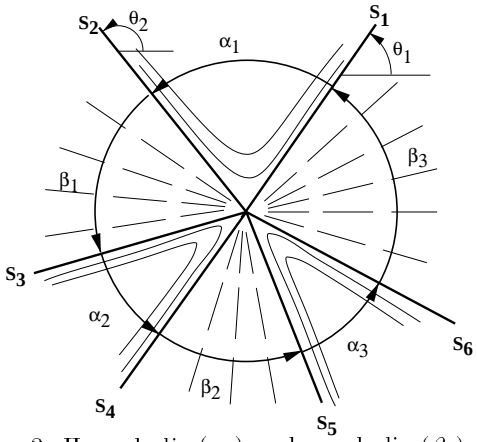

Figure 2: Hyperbolic (α_i) and parabolic (β_j) sectors at a degenerate point.

The index at the degenerate point $\overline{x}_0$ characterizes the pattern of neighboring hyperstreamlines. When traveling along a closed path encompassing $\overline{x}_0$, we encounter two types of angular sectors (Figure 2):

1 hyperbolic sectors α_i, where trajectories sweep past the degenerate point, and
2 parabolic sectors β_j, where trajectories lead away or towards the degenerate point.[2]

For example, the singularity in Figure 2 has three hyperbolic and three parabolic sectors. By analogy with vector fields, we call "separatrices" the dividing hyperstreamlines that separate one sector from the next, such as s_1 to s_6 in Figure 2. Let θ_k be the angle between the separatrix s_k and the x-axis. We show in Reference [7] that $x_k = \tan\theta_k$ must be a root of the cubic equation

$$dx^3 + (c+2b)x^2 + (2a-d)x - c = 0 \qquad (8)$$

Thus, there are at maximum three separatrices (real roots x_k) and *degenerate points have no more than three sectors.*

Consider a hypothetical singularity with n_p parabolic and n_h hyperbolic sectors ($n_p + n_h \leq 3$). The parabolic sectors span angles β_j ($j = 1, \ldots, n_p$) and the hyperbolic sectors span angles α_i ($i = 1, \ldots, n_h$). The eigenvectors rotate an angle β_j within a parabolic sector and $\alpha_i - \pi$ within a hyperbolic sector (Figure 2). Thus, during one counter-clockwise revolution around the degenerate point, the eigenvectors rotate an angle $2\pi I = \sum_{j=1}^{n_p}\beta_j + \sum_{i=1}^{n_h}(\alpha_i - \pi)$. Since $\sum_{j=1}^{n_p}\beta_j + \sum_{i=1}^{n_h}\alpha_i = 2\pi$, the index at the degenerate point is given by

$$I = 1 - \frac{n_h}{2}$$

It follows from Equation 7 that the number of hyperbolic sectors at a degenerate point is

$$n_h = 2 - sign(\delta)$$

[2] The reader familiar with sectors at critical points in vector fields may remember the existence of another type of sector called "elliptic" [8]. In the case of unsigned eigenvector fields, elliptic and parabolic sectors are indistinguishable and we group them in a unique parabolic class.

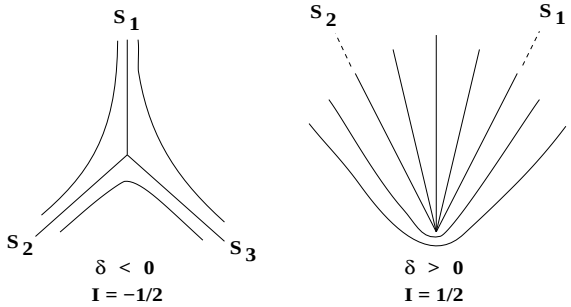

Figure 3: Trisector ($\delta < 0$) and wedge ($\delta > 0$) points. $\delta = ad - bc$ and I = index.

2.2 Trisector and wedge points

When $\delta < 0$, $n_h = 3$; the degenerate point has three hyperbolic sectors and, since $n_p + n_h \leq 3$, there is no parabolic sector. The pattern of hyperstreamlines corresponds to the *trisector point* shown by the texture[3] in Figure 6. See Figure 3 for a schematic depiction. We show in Reference [7] that each hyperbolic sector at a trisector point is less than 180^o wide.

When $\delta > 0$, $n_h = 1$; the degenerate point has one hyperbolic sector. The local pattern corresponds to the *wedge point* represented in Figures 6 and 3. We show in Reference [7] that the hyperbolic sector at a wedge point is always wider than 180^o. There are $n_p \leq 2$ parabolic sectors. When $n_p = 2$, the two parabolic sectors are contiguous and we combine them into a unique sector. Hence the pattern in Figure 3 where $n_p \leq 1$. (If $n_p = 0$, separatrices s_1 and s_2 are identical; the parabolic sector reduces to a single line.)

To summarize, *the most elementary singularities in tensor fields are trisector and wedge points. The invariant δ at the location of a degenerate point characterizes the nature of this point. $\delta < 0$ corresponds to a trisector point ($I = -\frac{1}{2}$) and $\delta > 0$ corresponds to a wedge point* ($I = \frac{1}{2}$). The crossing of the boundary $\delta = 0$ denotes a topological transition which we study in the next section. We defer until Section 3 a discussion of the global implications of the patterns delineated in Figure 3.

[3] We create the textures in this article and in the accompanying video by a technique discussed in References [7, 9].

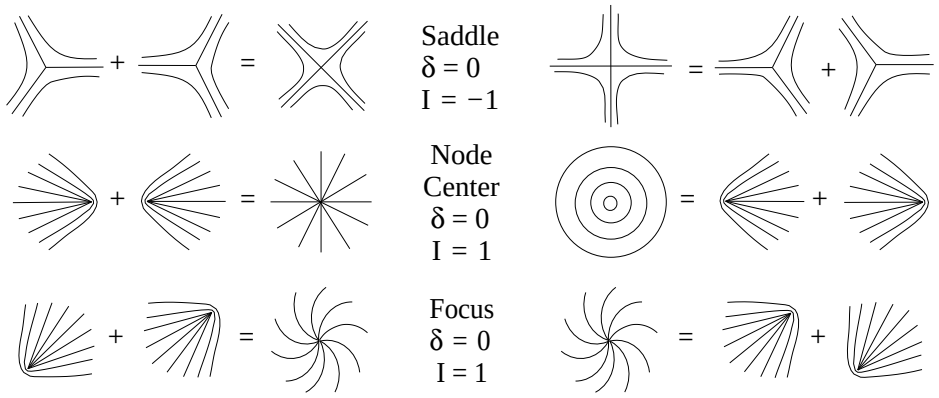

Figure 4: Merging degenerate points. δ = invariant given by Equation 6, I = index.

2.3 Merging degenerate points

Wedges and trisectors are stable structures in continuous tensor fields; they can not be broken into more elementary singularities with smaller index. In time-dependent flows, however, they move and can merge with each other, creating combined singularities of higher index.

A combination of degenerate points looks in the far field as a singularity whose index is the sum of the indices of its constituent parts. The following pattern, for example, is made up of 4 wedges and 2 trisectors. Its total index is $4 \times \frac{1}{2} - 2 \times \frac{1}{2} = 1$ and the structure looks indeed like a center ($I = 1$) in the far

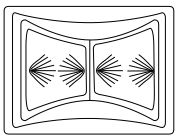

field. Figure 4 shows how merging trisectors create saddle points ($I = -\frac{1}{2} - \frac{1}{2} = -1$) and how merging wedges create nodes, centers, or foci ($I = \frac{1}{2} + \frac{1}{2} = 1$). Trisectors and wedges cancel each other by merging ($I = -\frac{1}{2} + \frac{1}{2} = 0$)—i.e., the singularity vanishes. Conversely, wedge-trisector pairs can be created from regular points. Pair creation is topologically consistent since it conserves the local index. (We show examples in Section 3.)

The merging of wedges and trisectors corresponds to $\delta = 0$. A more quantitative study of the patterns in Figure 4 is difficult since it requires developing tensor components at least to second order in Equations 5.

As opposed to critical points in vector fields, degenerate points with integral indices are usually unstable. They split into elementary wedges or trisectors soon after their creation by merging. They are nevertheless important for the study of instantaneous topologies.

3 Tensor Field Topology

We build on the theory of degenerate points to extract the topology of tensor fields and to study topological transitions.

The technique is similar to vector field topology with degenerate points playing the role of critical points. We represent each eigenvector field by a topological skeleton obtained by locating degenerate points and integrating the set of their connecting separatrices. We illustrate these concepts by visualizing the topology of the stress tensor in a 2-D periodic flow past a cylinder.

Fluid elements undergo compressive stresses while moving with the flow. Stresses are described mathematically by the stress tensor, which combines isotropic pressure and anisotropic viscous stresses. Both eigenvalues of the stress tensor are negative, and the two orthogonal eigenvectors, $\overline{v}_1$ and $\overline{v}_2$ (Equation 2), are along the least and the most compressive directions, respectively. At a degenerate point, the viscous stresses vanish and both eigenvalues are equal to the pressure; degenerate points are points of pure pressure.

The texture in Figure 7 shows the flow (velocity field) at one representative time step. The flow consists in the periodic detachment of a separation bubble. Overlaid are the degenerate points of the stress tensor.

□ **Video Clip 1** — The moving texture shows the flow evolving over time. Color encodes velocity magnitude from fast (red) to slow (blue).

3.1 Tracking degenerate points

The instantaneous representation in Figure 7 contains valuable information but we can learn more about the spatiotemporal structure of the tensor field by tracking the motion of degenerate points over time.

Figure 8 shows the trajectories followed by degenerate points in 3-D space. The third dimension is time,

increasing from front to back. The figure represents one period of the evolution of the flow. Red dots are wedge points and green dots are trisectors. C-events are creations of wedge-trisector pairs from regular flow, and M-events correspond to pair cancellation by merging.

In some instances, pair creations affect only the local flow; the two newly created points move together and eventually disappear by merging. Two C-events, however, are different; the newly created points move far away from each other, inducing a topological transition in the tensor field. These new wedge-trisector pairs are created periodically in a location alternatively above then below the cylinder symmetry axis. New wedge points are quickly dragged into the wake about the cylinder axis while new trisectors move downstream away from the axis.

□ **Video Clips 2 and 3** — We visualize the motion of degenerate points of the stress-tensor field. The colored background encodes the magnitude λ_2 of the most compressive force, from very compressive (red) to mildly compressive (orange, yellow, green) to little compressive (blue). We show wedge points as black dots and trisectors as white dots. Video Clip 2 represents the overall structure of the motion and Video Clip 3 focuses on the region closer to the body. The pair-creation events are clearly tight to each region of low compressive stresses (blue color).

3.2 Correlating vector and tensor data

Tensor data are highly multivariate and rich in information content but they are complex and poorly understood. Vector data are simpler and more familiar to scientists. It is useful to correlate visually tensor and vector fields, not only for our basic understanding of tensor data but also for gleaning new physical insights into vector fields.

□ **Video Clip 4** — The moving texture encodes the direction of the velocity field. Color encodes the magnitude of the most compressive eigenvalue λ_2. Overlaid are the degenerate points of the stress tensor.

Figure 7 represents one frame from this clip. Texture and color indicate clearly that detachment bubbles (saddle-center pairs of the velocity field) are regions of low compressive stresses. Red and white dots are wedge and trisector points of the stress tensor, respectively. The motion of the degenerate points is interesting. The wedge point A, which originated by pair creation, follows the detachment bubble in its motion downstream. In fact, a new pair is created with each new bubble. The oscillating pair B is closely associated to the recirculation regions close to the body surface. The wedge C follows a stable orbit shaped as an 8. It rolls back and forth between two consecutive bubbles without ever venturing inside.

3.3 Topological skeletons

We obtain topological skeletons by detecting degenerate points and integrating the set of their connecting separatrices.

Trisector points in tensor fields play the topological role of saddle points in vector fields. As shown in Figures 3 and 6, they deflect adjacent trajectories in any one of their three hyperbolic sectors toward topologically distinct regions of the domain. Wedge points possess both a hyperbolic and a parabolic sector. They deflect trajectories adjacent in their hyperbolic sector and terminate trajectories impinging on their parabolic sector.

Here follows an algorithm to extract the topology of a tensor field. This simplified version assumes that there are no merged degenerate points with integral index:

1 locate degenerate points by searching in every grid cell for solutions to Equations 3;

2 classify each degenerate point as a trisector ($\delta < 0$) or a wedge ($\delta > 0$) by evaluating a, b, c, d using Equations 4 and computing δ as in Equation 6;

3 select an eigenvector field;

4 use Equation 8 to find the three separatrices $\{s_1, s_2, s_3\}$ at each trisector point and the two separatrices $\{s_1, s_2\}$ at each wedge point (Figure 3); integrate hyperstreamlines along the separatrices; terminate the trajectories wherever they leave the domain or impinge on the parabolic sector of a wedge point.

Figure 9 shows an example. The texture represents the most compressive eigenvector of the stress tensor ($\overline{v}_2$). Color encodes as before the magnitude of the compressive force (λ_2), from most compressive (red) to least compressive (blue). We emphasize the structure of the tensor field by superimposing the topological skeleton of $\overline{v}_2$. The structure of these time-dependent data is very complex and we simplify the topology (in Figure 9 as in the remaining of this article) by computing only those separatrices that originate from trisector points, leaving on the side separatrices that emanate from wedge points.

We can mentally infer the orientation of the eigenvector at any point in the plane from the topological skeleton. Hyperstreamline trajectories curve so as to follow the shape of the separatrices, bending around wedge points.

With time, the repeated creation of new wedge-trisector pairs induces periodic topological transitions,

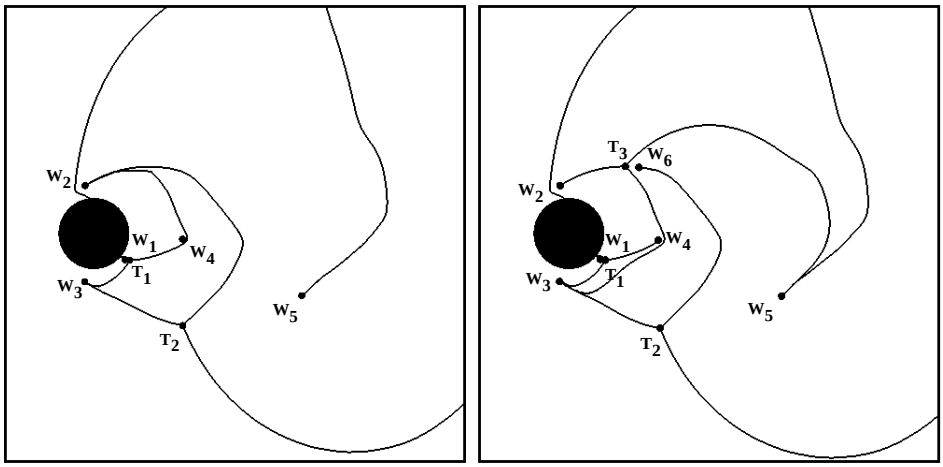

Figure 5: Two consecutive frames showing a topological transition of the stress-tensor field.

M	$\chi(\mathbf{M})$
sphere	2
torus	0
2-holed torus	-2
n-holed torus	2 - 2 n

Table 1: Euler characteristic of generic surfaces.

which we illustrate in Figure 5. The newly created pair $\{T_3, W_6\}$ changes the topological structure of the tensor field.

As with vector field topology, the power of the representation comes from its simplicity; a few points and lines suffice to reveal the directional information otherwise buried within abundant multivariate data.

□ **Video Clips 5 and 6** — The two clips show the evolution with time of the topological skeleton in Figure 9, with and without the textured background. Black dots represent wedge points and white dots are trisectors.

3.4 Trivariate data visualization

By using textures or topological skeletons, we render tensor information only partially. Indeed, we see from Equation 1 that 2D tensor data are truly trivariate. If the goal is to correlate full tensor information within a single display, one must visualize simultaneously two eigenvalues and the orientation of the eigenvectors.

In Figure 10, we use texture, color, and elevation as channels to encode eigenvector direction, longitudinal eigenvalue, and transverse eigenvalue, respectively.[4] In addition to topological information the display reveals a strong correlation between the two eigenvalues—a fact that was previously overlooked in representations such as Figures 5 and 9.

4 Tensor Topological Rule

When a tensor field is defined across a surface $\mathbf{M}$, the topology of $\mathbf{M}$ puts a constraint on the number and nature of degenerate points, limiting considerably the variety of possible tensor patterns. We investigate this constraint in this section.

The topology of any surface $\mathbf{M}$ is unambiguously characterized by a single number $\chi(\mathbf{M})$ called the surface's Euler characteristic [8]. All orientable[5] homeomorphic surfaces—i.e., the set of orientable surfaces that can be distorted to look identical by continuous bending, stretching, or squashing, but without tearing or gluing—have the same value of $\chi(\mathbf{M})$. For example, a sphere and a cube are homeomorphic with $\chi(\mathbf{M}) = 2$. A torus and a coffee mug are homeomorphic with $\chi(\mathbf{M}) = 0$. Table 1 lists $\chi(\mathbf{M})$ for a few generic surfaces.

A classical theorem of surface topology, known as the Poincaré-Hopf theorem [11], stipulates that the sum of the indices at the critical points of a vector field defined across a surface $\mathbf{M}$ is equal to $\chi(\mathbf{M})$. Thus, if such a vector field has $\mathcal{N}$ nodes, $\mathcal{C}$ centers, $\mathcal{F}$ foci, and $\mathcal{S}$ saddles, the total index is $\mathcal{N}+\mathcal{C}+\mathcal{F}-\mathcal{S} = \chi(\mathbf{M})$. This important result shows how the topology of the surface $\mathbf{M}$—i.e., $\chi(\mathbf{M})$—affects the structure of any vector field

[4] The vertical stretching creates an unwanted distortion of the texture which can be compensated for by techniques such as those described in Reference [10].

[5] See Reference [8] for a precise definition of surface orientability. Most of the surfaces in every day life are orientable. Notable exceptions include Möbius bands and Klein bottles.

defined across $\mathbf{M}$—i.e., $\mathcal{N} + \mathcal{C} + \mathcal{F} - \mathcal{S}$.

In order to extend the Poincaré-Hopf theorem from vector fields to tensor fields, we make the assumption that the sum of the indices at the degenerate points of a tensor field $\mathbf{T}(\overline{x})$ defined across the surface $\mathbf{M}$ depends only on the topology of $\mathbf{M}$ and *not* on the particular tensor field $\mathbf{T}(\overline{x})$. The following topological rule results:

Tensor topological rule — *Let $\mathbf{T}(\overline{x})$ be a tensor field defined across an orientable surface $\mathbf{M}$ having Euler characteristic $\chi(\mathbf{M})$. If $\mathbf{T}(\overline{x})$ has only isolated degenerate points consisting exclusively of $\mathcal{W}$ wedges, $\mathcal{T}$ trisectors, $\mathcal{N}$ nodes, $\mathcal{C}$ centers, $\mathcal{F}$ foci, and $\mathcal{S}$ saddles, then the sum of the indices at the degenerate points of $\mathbf{T}(\overline{x})$ is equal to $\chi(\mathbf{M})$. Hence the topological rule:*

$$\frac{1}{2}(\mathcal{W} - \mathcal{T}) + \mathcal{N} + \mathcal{C} + \mathcal{F} - \mathcal{S} = \chi(\mathbf{M}) \qquad (9)$$

We refer the reader to Reference [7] for a proof. As with vector fields, this rule establishes a connection between the topology of the surface $\mathbf{M}$—i.e., $\chi(\mathbf{M})$—and the structure of any tensor field defined across $\mathbf{M}$—i.e., the sum of indices.

Equation 9 restricts considerably the number of possible surface tensor patterns. For example, Figure 11 shows two complex tensor fields—one defined across a torus and another one across a sphere. A topological analysis reveals $\mathcal{N} = \mathcal{C} = \mathcal{F} = \mathcal{S} = 0$, $\mathcal{W} = \mathcal{T} = 18$ for the torus, and $\mathcal{N} = \mathcal{C} = 1$, $\mathcal{F} = 0$, $\mathcal{W} = \mathcal{T} = 3$ for the sphere. Both sets of values satisfy Equation 9 with $\chi(\textbf{torus}) = 0$ and $\chi(\textbf{sphere}) = 2$, respectively.

5 Extensions and Conclusions

We can extend the theory of degenerate points to 3-D symmetric tensor fields, which have three real eigenvalues and three orthogonal eigenvectors. At a degenerate point where two eigenvalues are identical, locally two-dimensional patterns such as wedges and trisectors (Figure 3) occur in the plane orthogonal to the third eigenvector. However, it remains to characterize the fully three-dimensional patterns that exist in the vicinity of degenerate points where three eigenvalues are identical.

The results presented above are also useful for unsymmetric tensor fields. We show in Reference [6] that it is always possible to extract a symmetric tensor component from unsymmetric data. We can then apply the topological analysis to the symmetric component for unveiling, at least partially, the structure of the tensor field.

In conclusion, visualization allowed us to elucidate the structure of symmetric tensor fields, demonstrating the tremendous potential of the field for building new knowledge beyond the usual goal of inspecting results from experiments and computations.

Acknowledgements

We are most indebted to Dan Asimov from NASA Ames for a useful discussion on topology, and to Mark Peercy from Stanford University for his critical comments and some of his software. The authors are supported by NASA under contract NAG 2-911 which includes support from the NASA Ames Numerical Aerodynamics Simulation Program and the NASA Ames Fluid Dynamics Division, and also by NSF under grant ECS9215145.

References

[1] T. Delmarcelle and L. Hesselink, "A unified framework for flow visualization," in *Computer Visualization* (R. Gallagher, ed.), ch. 5, CRC Press, 1994.

[2] J. L. Helman and L. Hesselink, "Visualization of vector field topology in fluid flows," *IEEE Computer Graphics and Applications*, vol. 11, no. 3, pp. 36–46, 1991.

[3] A. Globus, C. Levit, and T. Lasinski, "A tool for visualizing the topology of three-dimensional vector fields," in *Proc. IEEE Visualization '91*, pp. 33–40, 1991.

[4] A. I. Borisenko and I. E. Tarapov, *Vector and Tensor Analysis with Applications*. Dover Publications, New York, 1979.

[5] R. R. Dickinson, "A unified approach to the design of visualization software for the analysis of field problems," in *Proc. SPIE*, vol. 1083, pp. 173–180, SPIE, Bellingham, WA., 1989.

[6] T. Delmarcelle and L. Hesselink, "Visualizing second-order tensor fields with hyperstreamlines," *IEEE Computer Graphics and Applications*, vol. 13, no. 4, pp. 25–33, 1993.

[7] T. Delmarcelle, *The Visualization of Second-Order Tensor Fields*. PhD thesis, Stanford University, 1994. To be published.

[8] P. A. Firby and C. F. Gardiner, *Surface Topology*. Ellis Horwood series in Mathematics and its Applications, John Willey & Sons, New York, 1982.

[9] B. Cabral and L. C. Leedom, "Imaging vector fields using line integral convolution," *Computer Graphics (SIGGRAPH'93 Proc.)*, pp. 263–272, 1993.

[10] J. Maillot, H. Yahia, and A. Verroust, "Interactive texture mapping," *Computer Graphics (SIGGRAPH'93 Proceedings)*, vol. 27, pp. 27–34, 1993.

[11] J. W. Milnor, *Topology from the Differentiable Viewpoint*. The University Press of Virginia, Charlottesville, 1965.

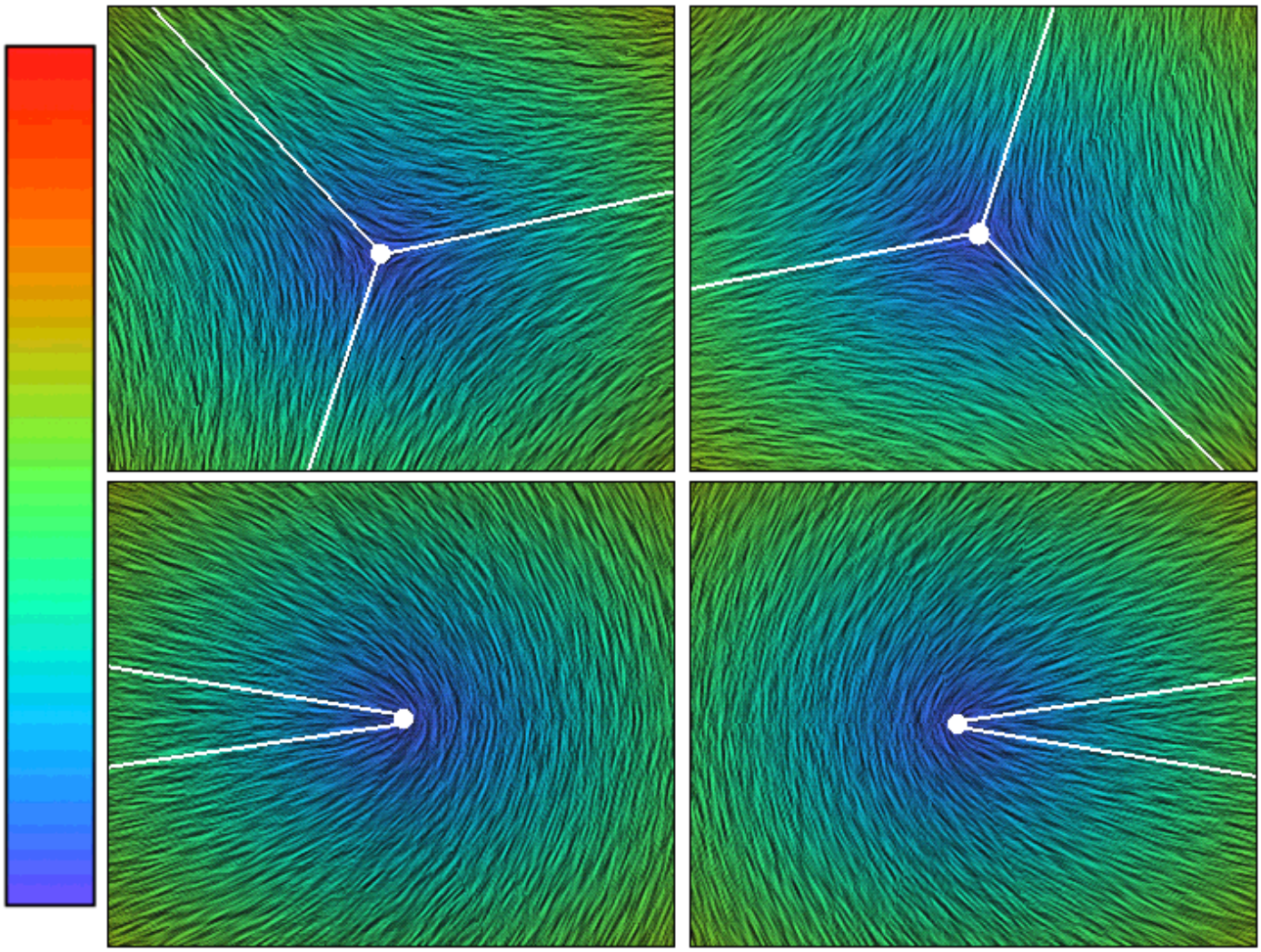

Figure 6: Textures representing the two eigenvector fields in the vicinity of a trisector point (top) and a wedge point (bottom). Color encodes the difference between the two eigenvalues.

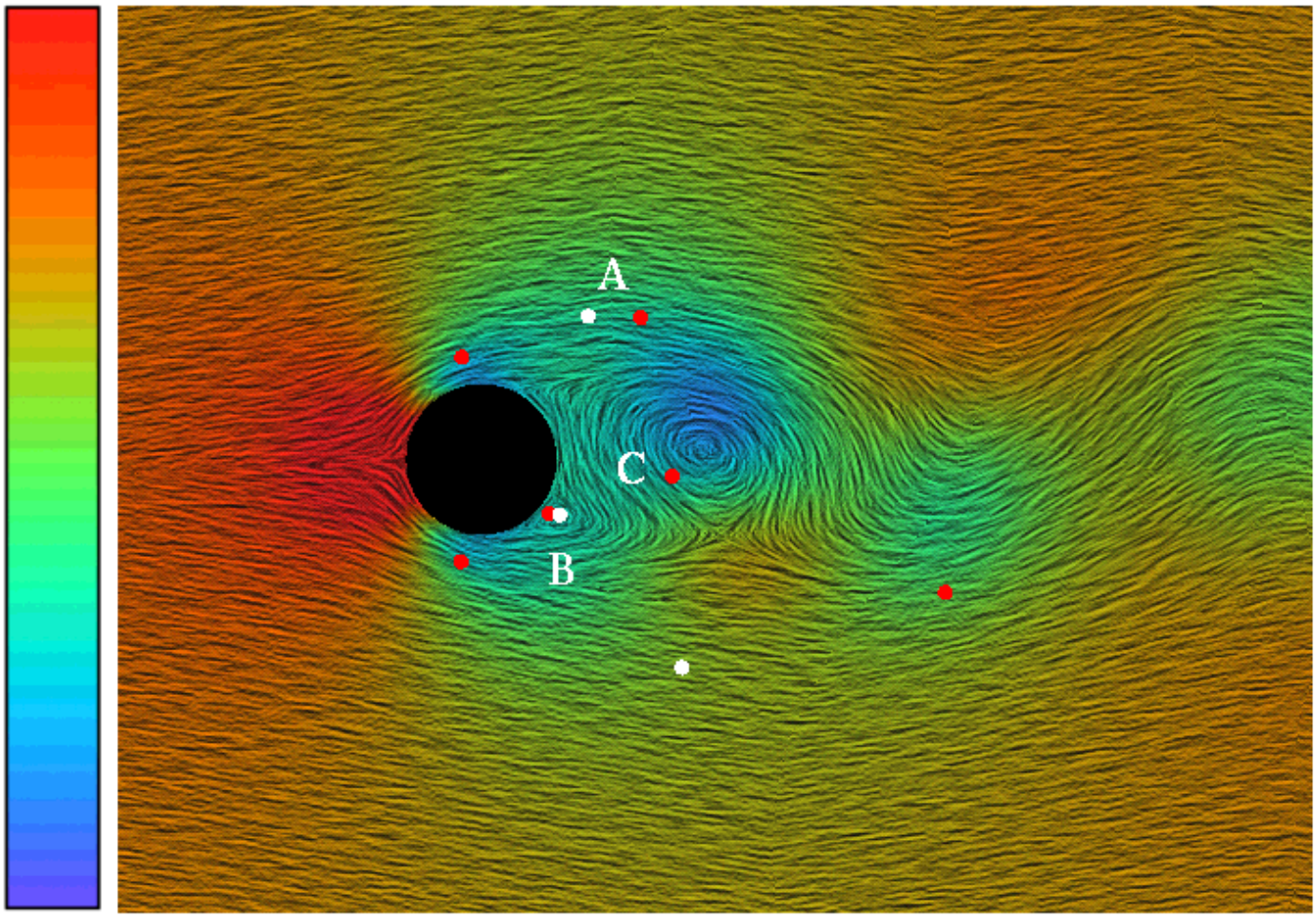

Figure 7: A frame of Video Clip 4 showing the correlation between the velocity field (moving texture) and the degenerate points of the stress tensor. Color encodes the most compressive stress. Red dots = wedges, white dots = trisectors. (See the video tape accompanying the Visualization '94 proceedings.)

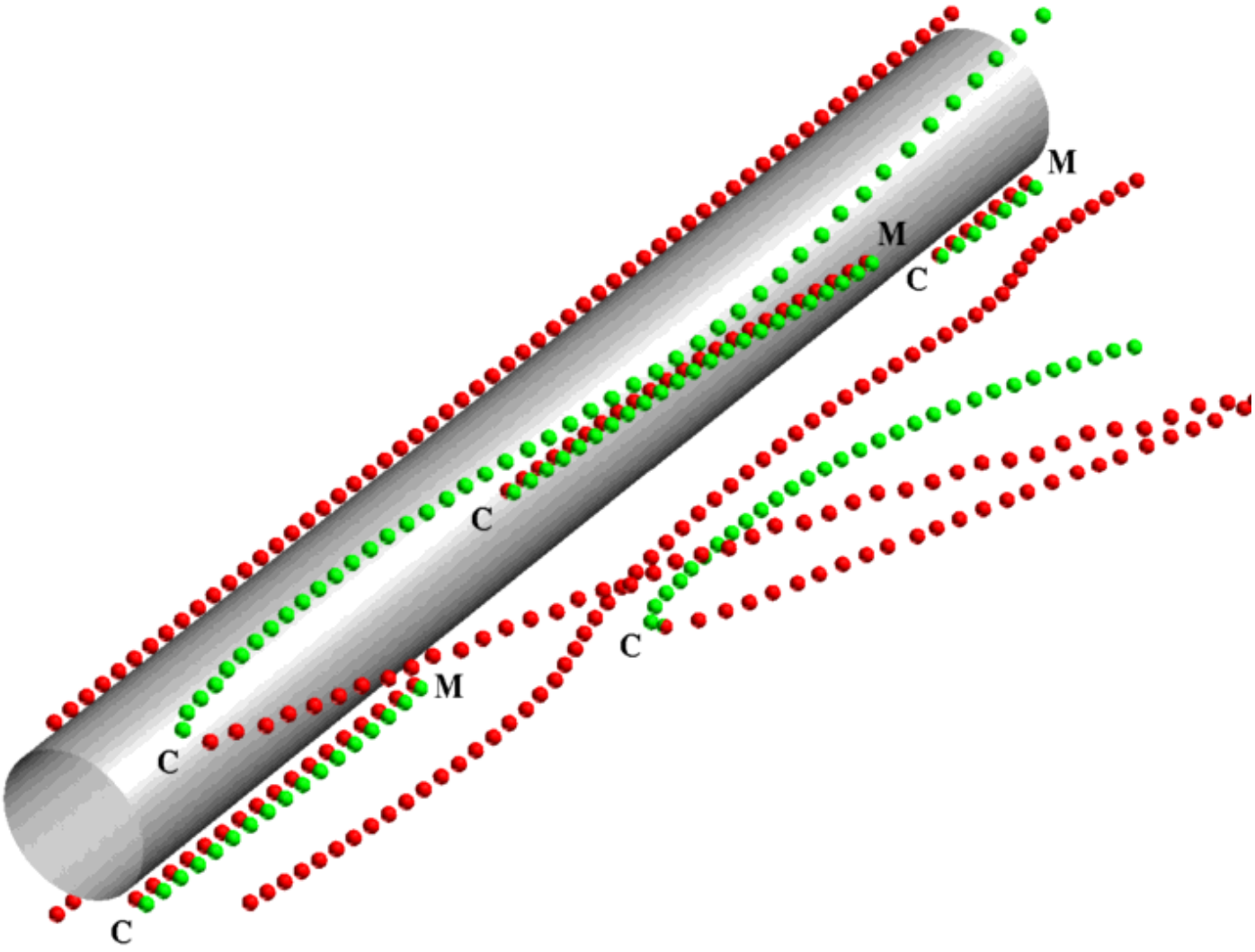

Figure 8: Spatiotemporal trajectories of degenerate points in the stress-tensor field. Time increases from front to back. Red spheres = wedges, green spheres = trisectors. M and C indicate merging and creation of wedge-trisector pairs, respectively. (See the video tape accompanying the Visualization '94 proceedings.)

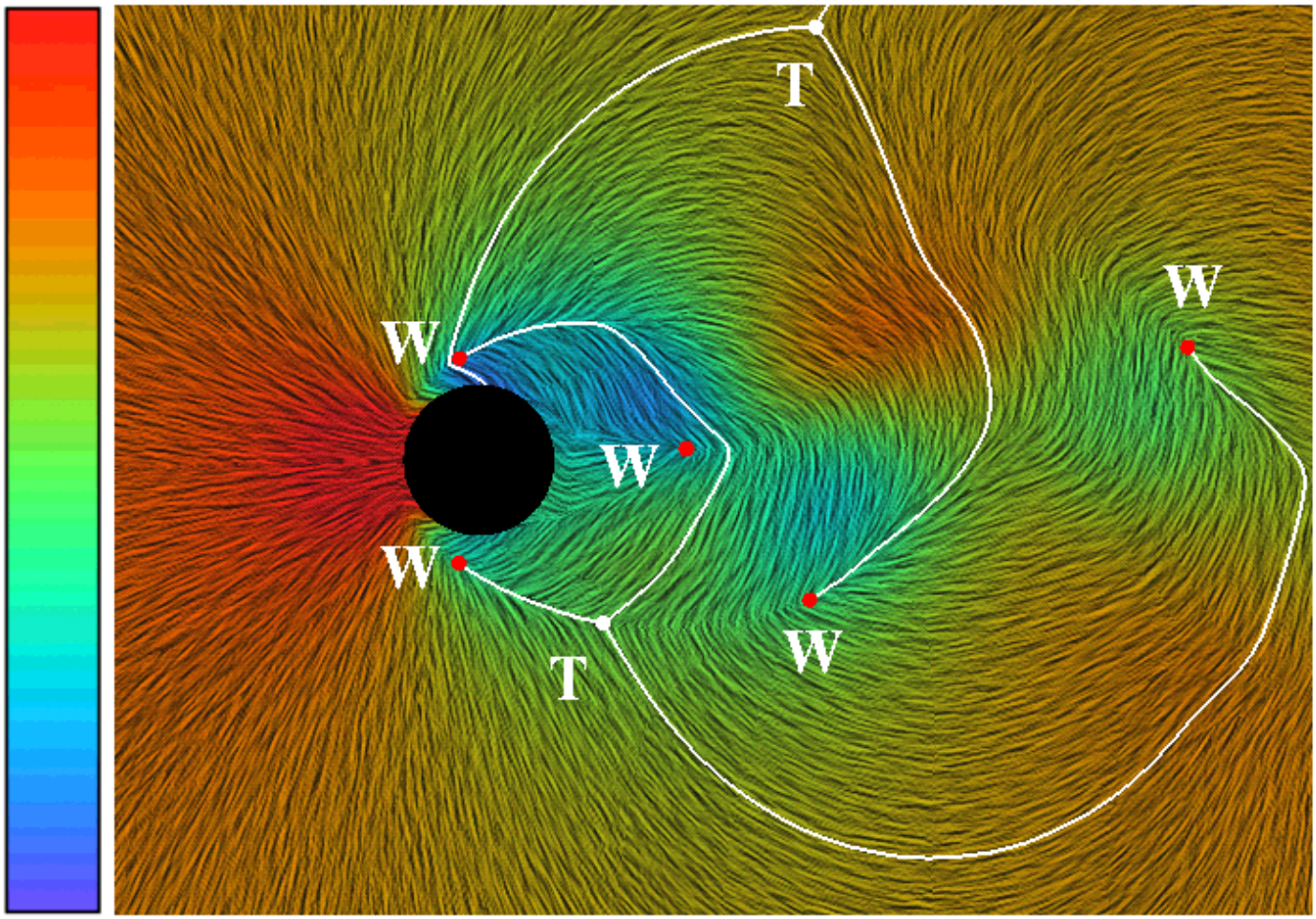

Figure 9: A frame of Video Clip 5 showing the instantaneous topology of the most compressive eigenvector $\overline{v}_2$. Color encodes λ_2. W = wedge, T = trisector. (See the video tape accompanying the Visualization '94 proceedings.)

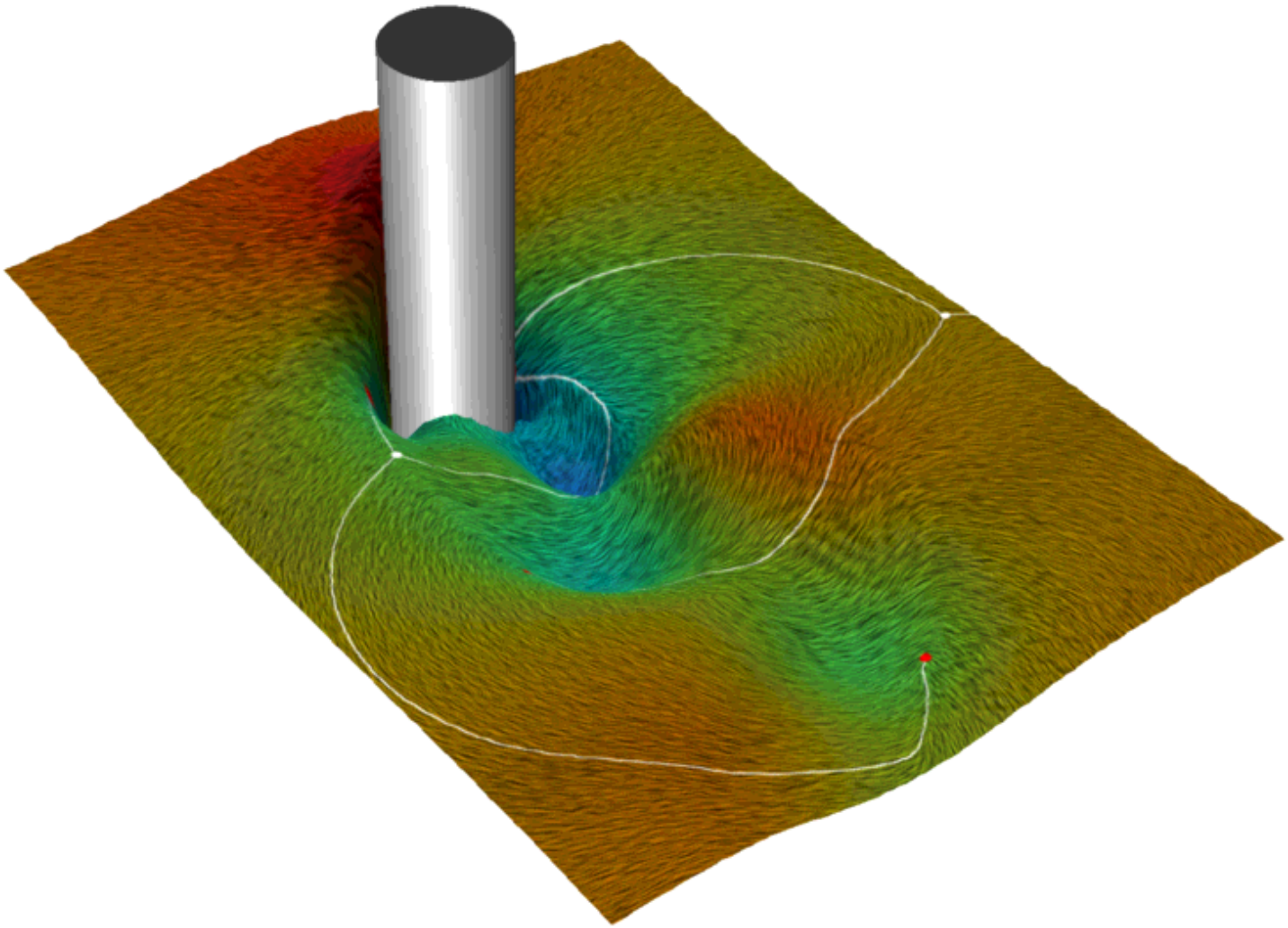

Figure 10: Trivariate data visualization to fully represent the stress-tensor field.

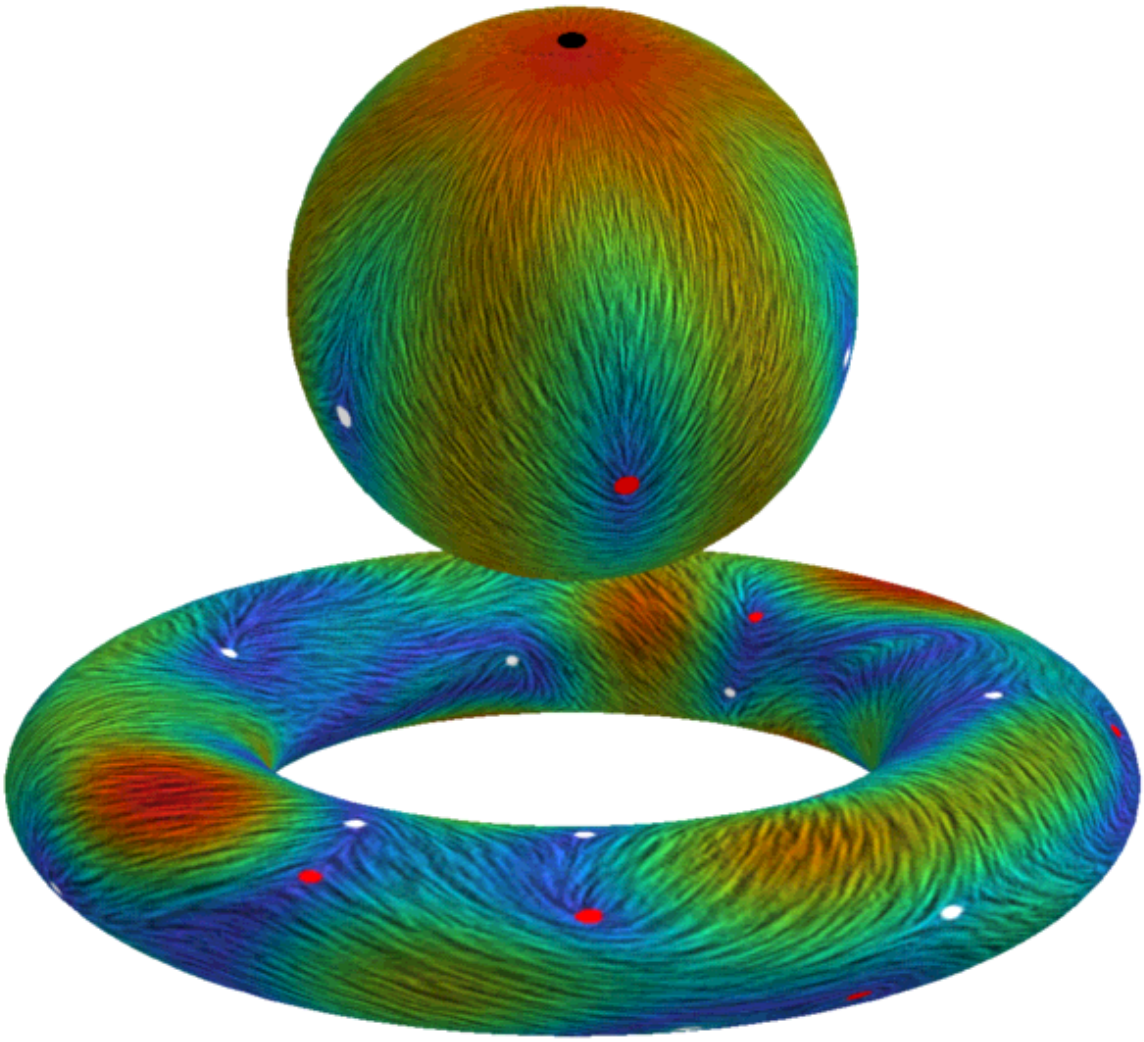

Figure 11: Illustration of the tensor topological rule for a torus and a sphere.